

---

# Isotopic Fractionation During Solidification of H<sub>2</sub>–HD–D<sub>2</sub> Mixtures

## Introduction

In inertial fusion experiments, it is energetically advantageous to form the fuel into a solid shell before compression.<sup>1</sup> Current cryogenic target experiments on OMEGA are being performed with pure deuterium (D<sub>2</sub>) as the fuel.<sup>2</sup> Future cryogenic target experiments will be performed with an equimolar solid mixture of deuterium and tritium (D-T). An equilibrium D-T mixture consists of D<sub>2</sub>, DT, and T<sub>2</sub> molecules in a 25:50:25% ratio. Each molecular species has a different triple point, which may lead to fractionation of the isotopes during fuel-layer formation. Spatial separation of the D and T nuclei due to isotopic fractionation during the cryogenic target layering process reduces the efficiency of the fusion reaction.<sup>3</sup>

Complete isotopic fractionation has long been predicted for hydrogen isotopes for temperatures approaching absolute zero—well below the triple point of the mixture.<sup>4</sup> It has been observed for <sup>3</sup>He–<sup>4</sup>He mixtures but not for bulk solid hydrogen isotope mixtures. Partial fractionation of hydrogen–deuterium mixtures has been observed in monolayers adsorbed onto graphite substrates using neutron scattering and x-ray diffraction.<sup>5</sup> The separation is mainly limited to the formation of local molecular clusters of one isotope versus the other as the monolayer is completed. It was speculated that no long-range ordering was observed because of the limited mobility of the molecules at temperatures approaching 3 K.

We have examined the possibility of fractionation in cryogenic targets using a 25:50:25% mixture of H<sub>2</sub>, HD, and D<sub>2</sub> (H-D). The use of nonradioactive hydrogen isotopes allows a simpler experimental system to be constructed without the radiological controls necessary for using tritium. Although nonradiological experiments are easier to perform, less fractionation may occur in samples containing tritium. Molecular diffusion in the bulk may be enhanced for D-T mixtures because of the large amount of energy deposited locally from  $\beta$  decay, which raises the neighboring solid's temperature and disassociates nearby molecular bonds. This study investigates fractionation that occurs during the liquid-to-solid phase transition near the triple point. Possible fractionation during

solid-to-vapor-to-solid mass transfer during  $\beta$ -layering or IR-enhanced  $\beta$ -layering as a result of sublimation and refreezing will be investigated in a future study.

For the liquid-to-solid phase transition, there was little separation of the isotopes during the solidification process. The maximum spatial concentration gradients are of the order of 0.02 to 0.05 molecular fraction per millimeter. The average D<sub>2</sub> concentration gradient (percentage) is greatest for the lowest D<sub>2</sub> concentrations. The absorption coefficient's gradient was also measured and appears to be less for the longer cooling times, which may be indicative of solid diffusion. Thermodynamically, the mixtures form a completely soluble isomorphous system since the mixture solidifies over a finite temperature range for all concentrations.

## Experimental Details

By scanning a focused infrared (IR) laser probe tuned to the major absorption band of D<sub>2</sub> at  $\tilde{\nu} = 3162 \text{ cm}^{-1}$  ( $\lambda = 3.162 \text{ }\mu\text{m}$ ) across a thin, slowly frozen solid sample of the mixture, the D<sub>2</sub> concentration as a function of position can be determined. The infrared absorption spectrum of pure deuterium is shown in Fig. 105.22. The major absorption peak of solid D<sub>2</sub> is from an induced dipole interaction between adjacent D<sub>2</sub> molecules in the crystal.<sup>7</sup> Solid hydrogen forms a hexagonal close-packed crystal at its vapor pressure. Therefore, each molecule has 12 nearest neighbors in the crystal, as shown in Fig. 105.23. Substitution of H<sub>2</sub> or HD into these sites will reduce the D<sub>2</sub>–D<sub>2</sub> dipole interaction and increase the local IR transmission.

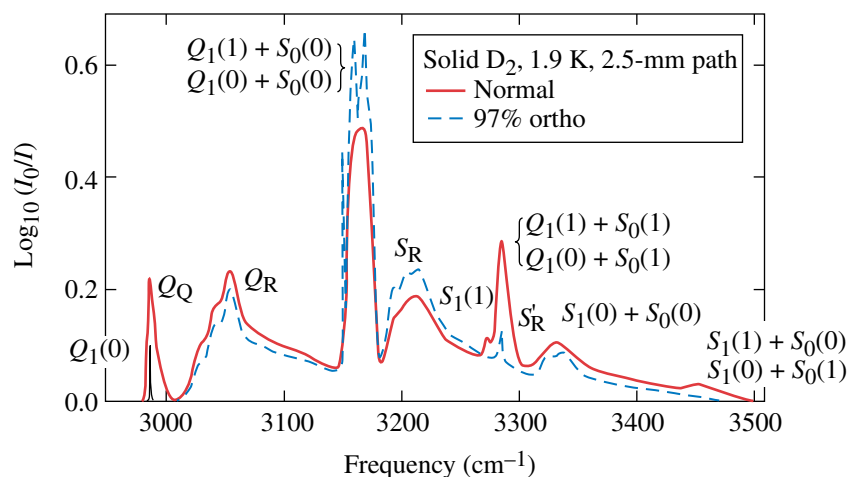
A schematic of the commercially available<sup>8</sup> infrared Pb:salt laser system is shown in Fig. 105.24. The IR laser diode is housed in a liquid-nitrogen (LN<sub>2</sub>) dewar and is operated at ~125 K and ~650 mA to produce an optical power approaching 1 mW at 3162 cm<sup>-1</sup>. The laser source is a PbSe double-hetero-structure, single-mode diode laser for high-resolution spectroscopy. It has a typical line width of  $6.7 \times 10^{-4} \text{ cm}^{-1}$ , a current tuning rate of 0.09 cm<sup>-1</sup>/mA, and a temperature tuning rate of 4 cm<sup>-1</sup>/K. This gives a wave number tuning range of ~3.140 to 3.190 cm<sup>-1</sup> over the operable temperature/current range. Even though the line

width is very narrow, by coarsely tuning the temperature and finely tuning the current, any wave number within the specified range can be achieved.

The light is collimated using an off-axis parabolic mirror which can be positioned in three dimensions. The light is sent through a grating monochromator that has been precalibrated to transmit only  $3.162 \pm 0.003$ - $\mu\text{m}$  light. The wavelength emitted by the laser diode is adjusted by varying its current at a fixed temperature until maximum transmission through the

monochromator is obtained. The dual-detector photodiode is also housed in a  $\text{LN}_2$  dewar. A small fraction ( $\sim 10\%$ ) of the beam is split off and focused onto one detector to monitor the stability of the laser source during data acquisition (refer to this as the reference beam).

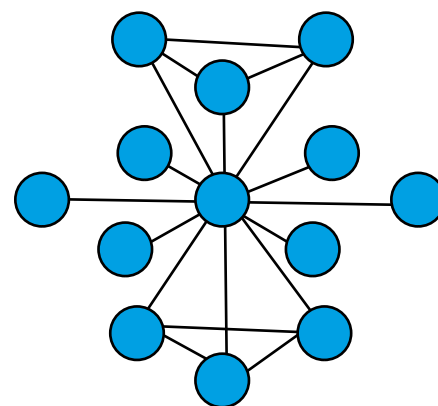
The remainder of the beam is transported through the sample. The light is focused to a  $0.3\text{-mm} \times 0.6\text{-mm}$  spot on the sample using an off-axis parabolic mirror mounted on a five-axis positioner. It is recollimated on the other side of the



T2067aJR1C

Figure 105.22

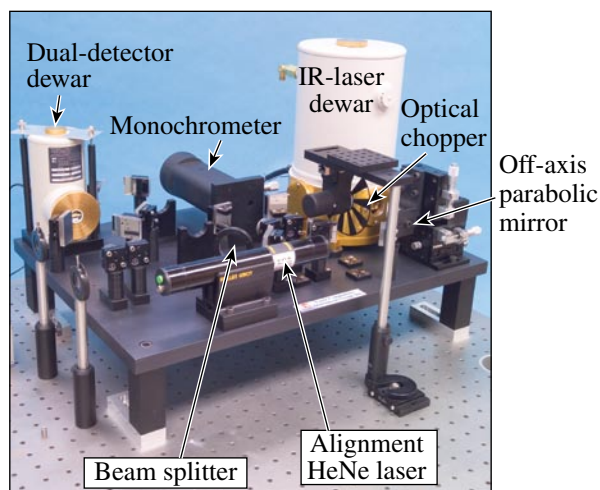
The absorption spectrum of solid  $\text{D}_2$  at 1.9 K for a 2.5-mm-thick sample. (Figure courtesy of the Canadian Journal of Physics.)<sup>6</sup>



T2067aJR2C

Figure 105.23

Each molecule in the hexagonal close-packed structure of solid hydrogen is neighbored by 12 other molecules. Substitution of non- $\text{D}_2$  molecules into these sites will interfere with adjoining  $\text{D}_2$ - $\text{D}_2$  dipole interactions and greatly reduce the absorption coefficient of the solid.



T2069JRC

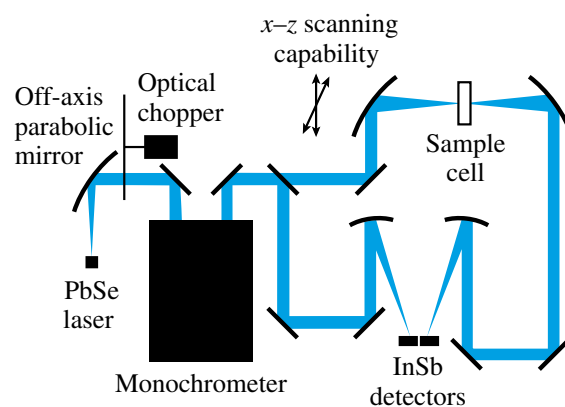


Figure 105.24

The optical layout and a schematic of the infrared Pb:salt laser system.

sample with an identical mirror and positioner. The mirrors are mounted on a stage that can be positioned with micrometer screws vertically and horizontally with respect to the fixed sample without causing the beam to “walk off” in the remainder of the optical system. This beam is subsequently focused onto the other detector (refer to this as the sample beam). The output of the IR laser is chopped at 790 Hz and the signals from each detector are sent to a chopper-synchronized lock-in amplifier with a 30-ms integration period.

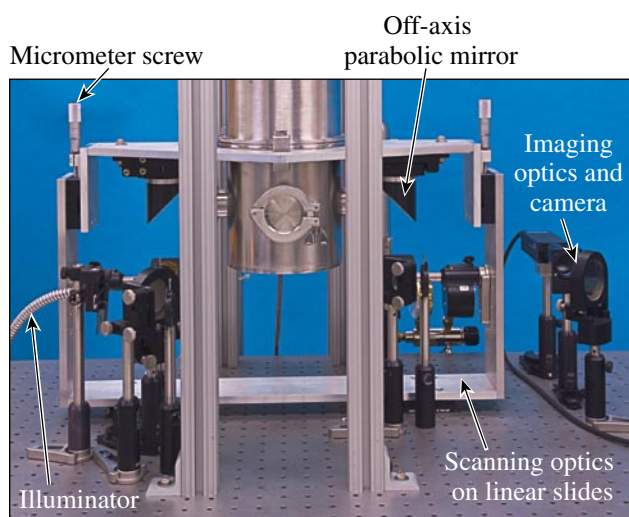
A sketch of the sample cell used to form the H-D crystal is shown in Fig. 105.25. The oxygen-free, high-conductivity copper cell is cooled from the bottom using a low-vibration Gifford-McMahon cryogenic refrigerator.<sup>9</sup> The cylindrical void that is filled with H-D is 6.4 mm in diameter by 3 mm thick; 2-mm-thick CaF windows are glued to either side of the copper cell. CaF was used instead of sapphire because of its lower thermal conductivity but similar IR transmittance at  $3.162\ \mu\text{m}$ . A heater and thermometer are attached to the top and bottom of the sample to produce a temperature gradient ( $\sim 0.5\ \text{K}$  maximum) across the sample.

The sample cell is loaded with liquid H-D through a 0.5-mm-diam stainless steel fill tube using a gas source pressure  $<10\ \text{psia}$ . For isotope mixtures, the sample cell is filled with just enough liquid to completely fill it before freezing to eliminate possible preferential condensation of the different isotopes from the gas-phase reservoir because of their different vapor pressures at a fixed temperature. This eliminates

the possibility of a concentration gradient forming because of the different vapor pressures of each isotope instead of from their different triple points. The cell remains connected to an external room-temperature gas source for isomolecular samples since they exhibit a single vapor pressure for each temperature, thus, the frozen sample completely fills the cell for these solid samples. The sample is cooled slowly (hours to days) by reducing the temperature at the top of the cell gradually to a value just below the final freezing temperature of the mixture.

Two flip-in mirrors are mounted before and after the parabolic mirrors. The first provides white-light illumination of the sample and the second sends the transmitted light to an imaging system with a CCD detector. This allows the sample to be viewed as the H-D solidifies. When examined between crossed linear polarizers, the crystal structure of the solid H-D is revealed (see example in Fig. 105.26). A HeNe laser beam can be made coaxial to the IR beam using a flip-in beamsplitter that allows visible alignment of the IR beam path. Using the second flip-in mirror alone with the HeNe beam, the focal spot of the IR beam can be located on the sample's image to provide beam position feedback.

The IR beam is raster scanned across the sample cell to determine if a  $D_2$  concentration gradient is present. The signal from the sample beam is recorded as a function of position at 0.5-mm increments. The signal from the reference beam is recorded periodically throughout the measurement to confirm the stability of the IR laser diode. (Typically, the output was sta-



T2071JRC

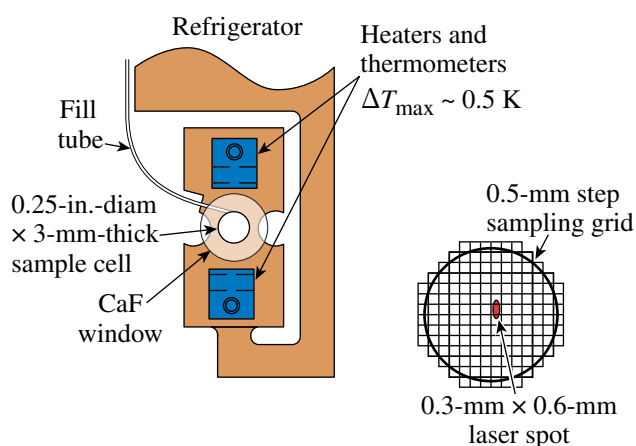


Figure 105.25

The scanning optics configuration and a sketch of the sample cell in which the H-D crystal is formed.

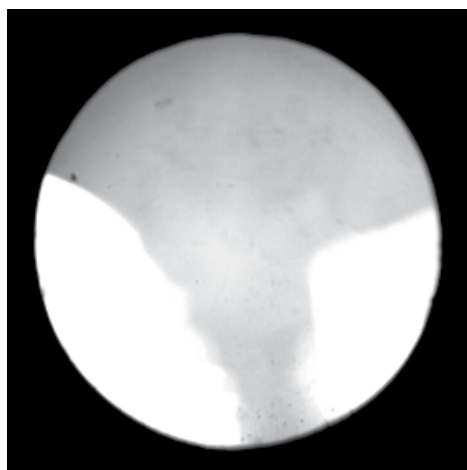


Figure 105.26

An image of a white-light, back-illuminated, solid pure D<sub>2</sub> sample. The crystal structure of the solid is revealed when examined between crossed linear polarizers; three distinct crystallites can be seen. The sample was frozen by reducing the temperature at the top of the sample from 19.2 K to 18.7 K over a 20-h period. The sample began to freeze at a bottom temperature of 18.7 K.

ble to <2% for the duration of the measurement.) The sample is subsequently vaporized at 30 K and the signal from the sample beam is recorded as a function of position for the empty cell. The two measurements are ratioed to create a transmission plot  $T(x,z)$ , as shown in Fig. 105.27(b). The absorption coefficient  $\alpha(x,z)$  is calculated from Beer's Law and includes a correction for the change in refractive index of the sample cell's contents with the solid present and absent (see appendix, p. 33).

## Results

The transmission plot of the 25:50:25% H<sub>2</sub>:HD:D<sub>2</sub> mixture, along with that of a pure D<sub>2</sub> sample, is shown in Fig. 105.27. (The mean absorption coefficient for each sample is given in Fig. 105.29.) Note that  $\alpha$  for the H-D mixture is  $\sim 1/20$ th of that for the pure D<sub>2</sub>. This reduction is disproportionate to the reduction in D<sub>2</sub> nearest neighbors—from 12 to 3 in the hexagonal close-packed crystal. In fact, the 3-mm-thick H-D mixture is >96% transmissive even though one in four molecules is D<sub>2</sub>. In contrast, a pure D<sub>2</sub> sample is only 40% transmissive. This is attributed to the simultaneous transition absorption requirement of two neighboring D<sub>2</sub> molecules, each absorbing a portion of the incident quantum.<sup>10</sup> Therefore, the interference of non-D<sub>2</sub> molecules between adjacent D<sub>2</sub> molecules greatly reduces the absorption coefficient of the bulk material. Any gradient present in this H-D transmission plot is easily masked by the noise in the data. The sensitivity of the D<sub>2</sub> absorption coefficient to concentration must first be resolved before a change in absorption can be quantified as a concentration gradient.

(a) H-D transmission

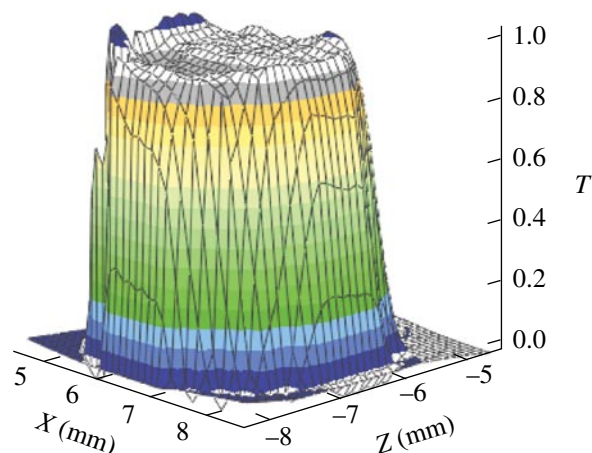
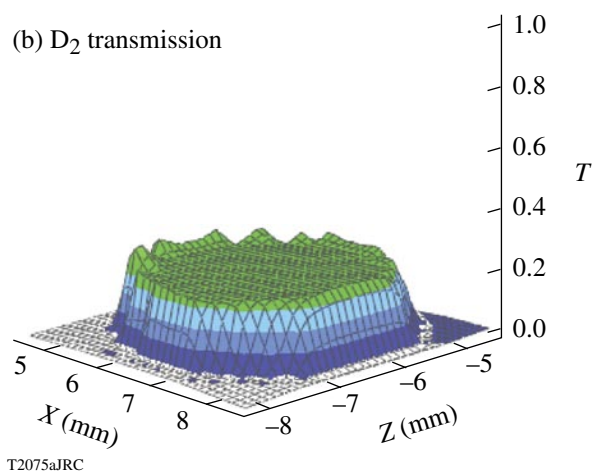
(b) D<sub>2</sub> transmission

Figure 105.27

Typical transmission plots for (a) 25:50:25% H<sub>2</sub>:HD:D<sub>2</sub> and (b) pure D<sub>2</sub>. The absorption coefficients are 0.017 and 0.317 mm<sup>-1</sup>, respectively; a 20× difference for a factor of 4 difference in D<sub>2</sub> concentration that is clearly outside the linear region of Beer's Law.

Beer's Law follows a linear relationship between the absorption coefficient and solute concentration for low concentrations (<10%). At these relatively high concentrations of D<sub>2</sub> in the H-D mixture (25% < D<sub>2</sub> < 100%), however, nonlinear deviations from Beer's Law are expected. The absorption coefficient of the D<sub>2</sub> in the H-D is a function of the D<sub>2</sub> intermolecular distance<sup>11</sup> as follows:

$$\alpha(\omega) \propto \sum_{nn'} (P_n - P_{n'}) \left| \langle n' | \mu | n \rangle \right|^2 \delta(\omega - \omega_{nn'}),$$

where  $\omega = 2\pi c/\lambda$  is the angular frequency of the incident radiation,  $P_n$  is the probability of occupancy of state  $n$  ( $P_n$  corresponding to absorption and  $P_{n'}$  to spontaneous emission),  $\mu$  is the dipole moment of the molecule, and  $\delta(\omega - \omega_{nn'})$  is the

Dirac delta function centered at the resonant frequency  $\omega_{nm}$ . The dipole moment  $\mu$  is proportional to  $Q_{\text{internuclear}} + Q_{\text{eqq}}$ , however, where  $Q_{\text{internuclear}}$  is related to a van der Waal's interaction and  $Q_{\text{eqq}}$  is the electric quadrupole-quadrupole interaction which varies as  $1/r_e^4$ , where  $r_e$  is the D<sub>2</sub> intermolecular distance. The intermolecular distance between D<sub>2</sub> molecules in the H-D mixture is inversely proportional to the D<sub>2</sub> concentration. Therefore, by plotting the absorption coefficient of the D<sub>2</sub> in the H-D mixture as a function of the D<sub>2</sub> fraction in the mixture, the slope can be used to quantify a transmission gradient as a concentration gradient.

A variety of H<sub>2</sub>-D<sub>2</sub> mixtures were solidified at varying rates and their  $\alpha(x,z)$  measured. Three to seven individual samples were frozen and measured for each mixture to obtain adequate statistics. The transmission data is fit to a plane to determine the average transmission and the transmission gradient, as shown in Fig. 105.28. The resulting average absorption coefficient of the D<sub>2</sub> in the H-D mixture (at  $\lambda = 3.151 \mu\text{m}$ ) is plotted as a function of the D<sub>2</sub> molecular fraction  $f_{\text{D}_2}$  in Fig. 105.29. The function that best fits the data is

$$\alpha(f_{\text{D}_2}) = \exp(4.20 \times f_{\text{D}_2} - 5.26) \text{mm}^{-1}.$$

Conversely, to find the D<sub>2</sub> molecular fraction from the mean absorption coefficient

$$f_{\text{D}_2} = \frac{[\ln(\alpha \times 1 \text{ mm}) - 5.26]}{4.20}. \quad (1)$$

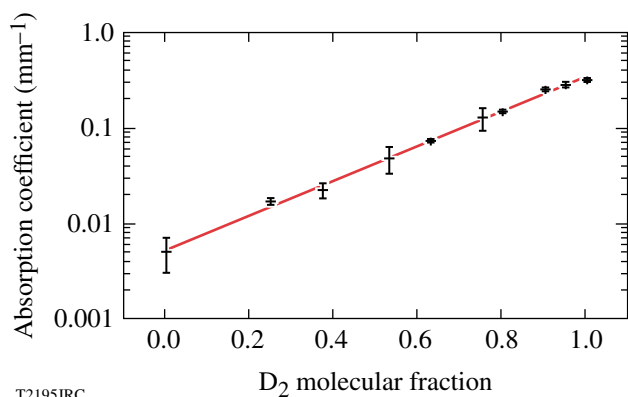


Figure 105.29

The average absorption coefficient of the D<sub>2</sub> in the H-D mixture as a function of the D<sub>2</sub> molecular fraction at an IR diode wavelength of  $\lambda = 3.151 \mu\text{m}$ . The vertical error bars indicate  $\pm 1$  standard deviation of the various experimental runs that were averaged for each point. The results from pure H<sub>2</sub> and D<sub>2</sub> samples are included for completeness. The finite absorption coefficient for H<sub>2</sub> indicates the scattering baseline of the experiment.

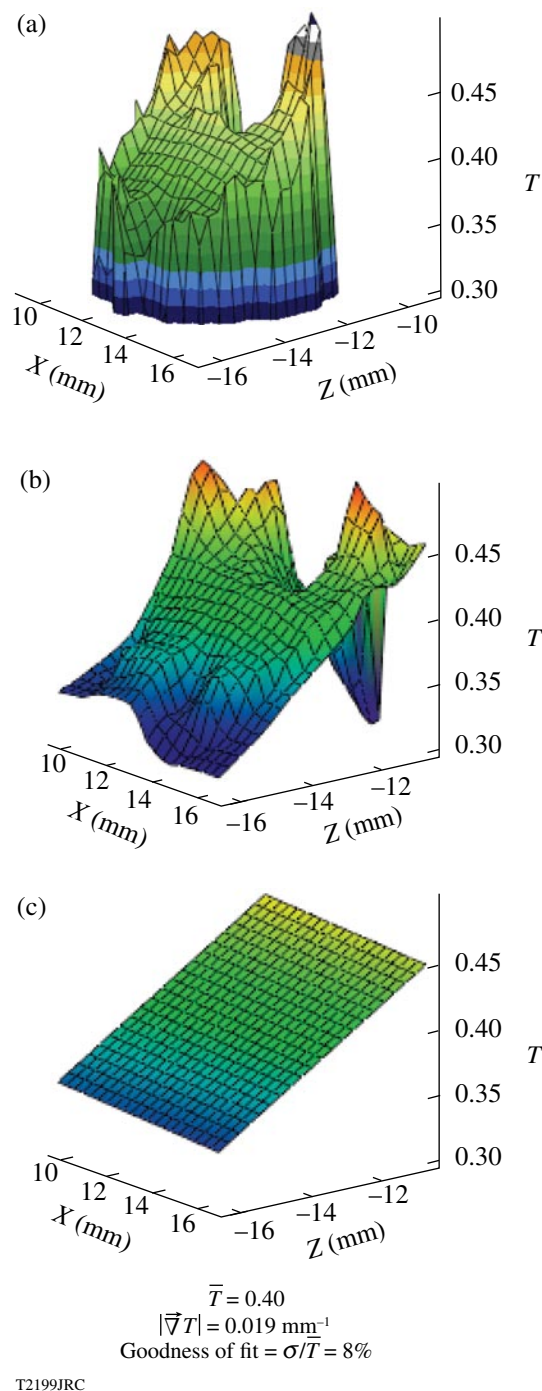


Figure 105.28

The transmission plots are processed from the raw data shown in (a) by first eliminating spurious data points to produce the plot in (b) and then fitting it to a plane, as shown in (c), to subsequently determine the D<sub>2</sub> concentration gradient. The hole at the top of the data is formed during solidification because of the large difference between the liquid and solid densities of hydrogen since the sample cell is filled with just enough liquid to completely fill it before freezing commences.

A plot of the absorption coefficient gradient as a function of freeze time is shown in Fig. 105.30. The samples were generally measured <2 h following solidification. The absorption coefficient gradient appears to be inversely proportional to the cooling time, but there is a large scatter in the data—especially for the shorter cooling times. This may be evidence of molecular diffusion in the bulk solid. Molecular diffusion between adsorbed H-D monolayers on graphite has been observed<sup>5</sup> to be of the order of  $5 \times 10^{-6}$  cm<sup>2</sup>/s near the triple point (17 K). This value increases by an order of magnitude at 30 K for adsorbed monolayers, but this temperature obviously cannot be obtained in the unpressurized solid. Molecular diffusion in the bulk may be enhanced for D-T mixtures because of the large amount of energy (~12 keV average) deposited locally from  $\beta$  decay, thus raising the neighboring temperature and disassociating molecular bonds.

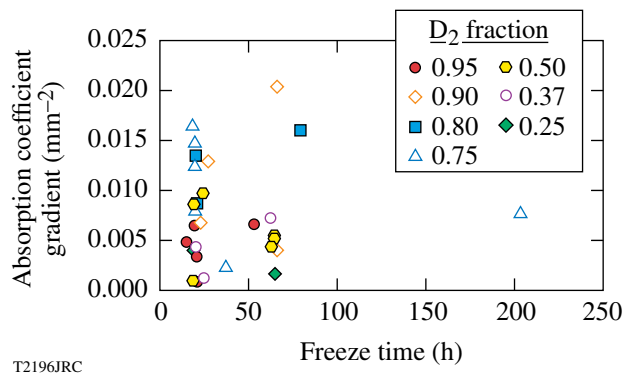


Figure 105.30

The absorption coefficient gradient as a function of freeze time. The vertical groupings indicate that most cooldowns were performed either over ~24 h or over ~72 h. A single long-duration cooldown is shown at the right of the figure. A few anomalous points occur at the top of the figure that may be indicative of IR scattering in the raw transmission data for these points.

It may be argued that scattering sites in the bottom of the sample are producing the apparent concentration gradient. These could originate from the large temperature excursion that the bottom of the sample undergoes during the freezing of the entire sample and the subsequent thermal contraction creating microcracks. This hypothesis is not supported by a plot of the absorption coefficient gradient as a function of initial bottom minus final top temperature (Fig. 105.31). In fact, observable cracks and striations do appear in the sample during the freeze duration but generally anneal out during the course of solidification. In addition, the absorption coefficient gradients for samples of individual isotopes are  $\sim 10^{-4}$  1/mm<sup>2</sup>—several orders of magnitude less than those for the mixtures—indicating that no scattering-induced gradients are present.

The average percentage  $D_2$  concentration gradient ( $\Delta f_{D_2}/\Delta z \times 1/f_{D_2}$ ) is greatest for the lowest concentrations, as shown in Fig. 105.32. Among the samples tested, however, the absolute concentration gradients ( $\Delta f_{D_2}/\Delta z$ ) are of the order of 0.02 to 0.05 mm<sup>-1</sup>. The large error bars shown for the lowest concentrations indicate the signal-to-noise ratio in the measurement is smallest when the sample is the least absorptive. This is another reason why the data in Fig. 105.29 are most useful

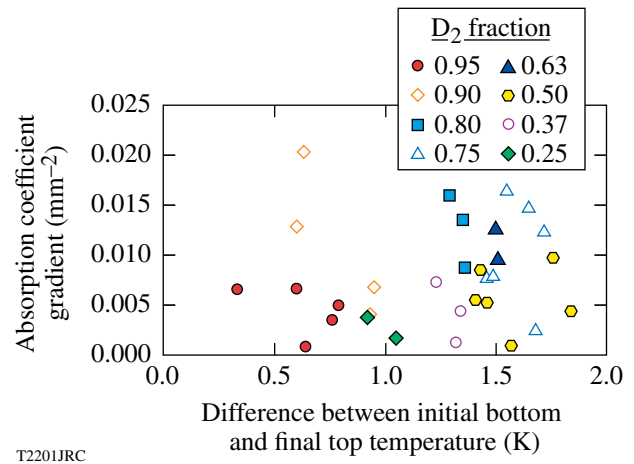


Figure 105.31

A plot of the absorption coefficient gradient as a function of the difference between the initial bottom and the final top temperature. If the gradient observed was due to increased IR scatter in the lower portion of the sample from microcracks, the trend in the data should be diagonal from bottom left to upper right. The data does not reflect this and is more or less randomly distributed.

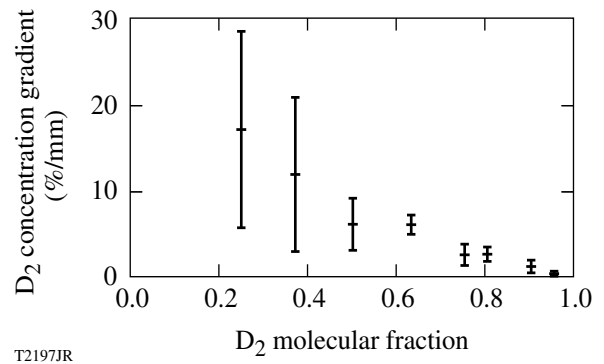


Figure 105.32

The average percentage  $D_2$  concentration gradient in the H-D mixture as a function of the  $D_2$  molecular fraction. The vertical error bars indicate  $\pm 1$  standard deviation of the various experimental runs that were averaged for each point and are greatest for the lowest concentrations since the signal-to-noise ratio is smallest for the least absorptive samples. The absolute concentration gradients are of the order of 0.02 to 0.05 molecular fraction mm<sup>-1</sup>.

Table 105.I: Calculated first-freezing temperatures for the 25:50:25% H<sub>2</sub>:HD:D<sub>2</sub> mixture using Eq. (2). Molecular fractions are based on both the pressurization schedule of the gas reservoir when the sample was prepared and on an independent measurement of the sample using cryogenic gas chromatography. The final column is the first-freezing temperature of the remaining 33:67% H<sub>2</sub>:HD mixture if the D<sub>2</sub> completely froze out of the solution first.

Molecule	Triple point (K)	Mass fraction from pressure	Mass fraction from mass spectrometer	Mass fraction with frozen D <sub>2</sub>
H <sub>2</sub>	13.96	0.249±0.005	0.26±0.02	1/3
HD	16.60	0.495±0.005	0.50±0.02	2/3
D <sub>2</sub>	18.73	0.256±0.005	0.24±0.02	0
	First-freezing temperature (K)	16.49	16.42	15.72

Experimentally, the first-freezing temperature for the frozen mixture was 16.53 K and the mixture had completely frozen at ~16 K. This implies that complete fractionation does not occur in the mixture.

for extrapolating the D<sub>2</sub> concentration gradient present in a weakly absorbing 25:50:25% mixture of H<sub>2</sub>, HD, and D<sub>2</sub> from more absorptive mixtures.

Another indication that significant fractionation does not occur in a H-D mixture is the thermodynamic properties of the solidification process. Each H-D mixture does not have a specific triple point but exhibits a first-freezing temperature and solidifies over a finite temperature range. First, consider the 25:50:25% mixture of H<sub>2</sub>, HD, and D<sub>2</sub>. The temperature at which the mixture begins to freeze (i.e., the first-freezing temperature)  $\theta$  is given by

$$\theta = \sum_i (f_i \times T_{p,i}), \quad (2)$$

where  $f_i$  and  $T_{p,i}$  are the molecular fraction and triple point of the  $i^{\text{th}}$  component, respectively. Values for this mixture are shown in Table 105.I. Molecular fractions in the table are based on both the pressurization schedule of the gas reservoir when the sample was prepared and on an independent measurement of the sample using cryogenic gas chromatography.<sup>12</sup> Experimentally, the first-freezing temperature for the mixture was 16.53 K and the mixture had completely frozen at ~16.1 K. This implies that complete fractionation does not occur in the mixture since the H<sub>2</sub> fraction would not have begun to freeze until 13.96 K. Indeed, if the D<sub>2</sub> had initially frozen out of solution, the remaining HD-H<sub>2</sub> mixture would not have begun to freeze until 15.72 K, well below the 16.1 K experimentally determined last-freezing temperature.

The first- and last-freezing temperatures were measured for each H-D mixture. As the temperature at the top of the sample was reduced, the highest temperature at the bottom of the

sample at which crystallites began forming was recorded as the first-freezing temperature. Likewise, the highest temperature at the top of the sample at which the sample had completely frozen was recorded as the last-freezing temperature. The data points are shown in Fig. 105.33. This plot is indicative of a classic completely soluble isomorphous system.<sup>13</sup> Such behavior is not unreasonable since the chemical, and therefore crystallographic, nature of each isotope is identical.

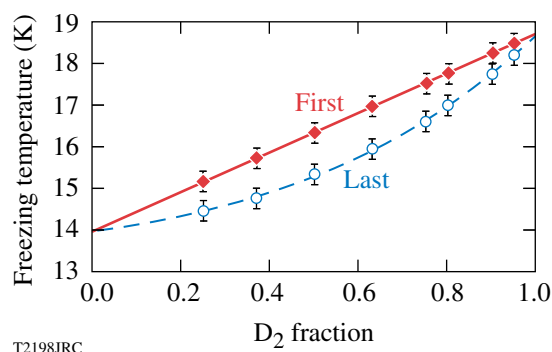


Figure 105.33

The experimentally measured first- and last-freezing temperatures (diamonds and circles, respectively) indicate that the H-D mixtures form a completely soluble isomorphous system. The upper line is from Eq. (2) and uses the known concentration of each mixture and the triple point of each molecule. The lower curve is a third-order least squares polynomial fit to the experimental data. The error bars indicate the  $\pm 50$  mK uncertainty in the measured temperatures.

## Conclusions

The average absorption coefficient of the D<sub>2</sub> in a H<sub>2</sub>-D<sub>2</sub> mixture was measured as a function D<sub>2</sub> molecular fraction. The absorption coefficient varies exponentially with D<sub>2</sub> concentration. This is expected since the relatively large concentrations of D<sub>2</sub> in the H-D mixture used in this study deviate from the

low-concentration linear regime over which Beer's Law is valid. There was little separation of the isotopes during the solidification process. The maximum spatial concentration gradients are of the order of 0.02 to 0.05 molecular fraction per millimeter. The average D<sub>2</sub> concentration gradient (percentage) is greatest for the lowest concentrations. The absorption coefficient's gradient was also measured and appears to be inversely proportional to the cooling time, which may be indicative of solid diffusion. Thermodynamically, the mixtures form a completely soluble isomorphous system since the mixture solidifies over a finite temperature range for all concentrations. Possible fractionation during solid-to-vapor-to-solid mass transfer as a result of sublimation and refreezing will be investigated in a future study.

Another observation is that the absorption coefficient for deuterium in the 25:50:25% H<sub>2</sub>:HD:D<sub>2</sub> mixture is nearly *twenty times lower* (0.017 mm<sup>-1</sup> versus 0.317 mm<sup>-1</sup> for pure D<sub>2</sub>). This is attributed to the simultaneous transition absorption requirement of two neighboring D<sub>2</sub> molecules. Therefore, the interference of non-D<sub>2</sub> molecules between adjacent D<sub>2</sub> molecules makes the 3-mm-thick H-D mixture >96% transmissive even though one in four molecules is D<sub>2</sub>. Compare this with a 40% transmission for a pure D<sub>2</sub> sample. This will greatly increase the time necessary to layer a D-T-filled capsule using IR-enhanced β-layering versus IR layering with pure D<sub>2</sub> using an IR laser tuned to the 3162 cm<sup>-1</sup> absorption band of D<sub>2</sub>.<sup>14</sup> One solution is to pump the DT molecule at 2888 cm<sup>-1</sup>, the wave number for the peak absorption for DT.<sup>15</sup> In comparison to 25% D<sub>2</sub>, DT makes up 50% of the D-T mixture and, extrapolating the data in Fig. 105.29 to similar behavior with DT concentration, will absorb significantly more IR radiation than the D<sub>2</sub> in the mixture.

## Appendix

The Beer-Lambert Law takes on various forms:  $A = \alpha'tc$ ,  $I_t/I_0 = e^{-\alpha'tc}$ , and  $A = \log(I_0/I_t)$ , with  $\alpha = \alpha'c = 4\pi k/\lambda$ , where  $A$  is the absorbance,  $I_0$  is the intensity of the incident light,  $I_t$  is the intensity after passing through the material,  $t$  is the distance that the light travels through the material (i.e., the path length),  $c$  is the concentration of absorbing species in the material (mole solute per mole solvent),  $\alpha'$  is the molar absorption coefficient,  $\alpha$  is the bulk absorption coefficient,  $\lambda$  is the wavelength of the light, and  $k$  is the extinction coefficient. In this treatment, since  $\alpha$  is a strong nonlinear function of concentration, it will be used instead of the molar absorption coefficient.

The transmission data must be corrected to account for the change in reflectivity of the sample cell upon vaporization of

the solid hydrogen sample. Incorporating Beer's Law above, the transmitted intensity  $I_t$  with the solid in the sample cell is given by

$$I_t = I_0 T_1^4 T_2^2 T_3^2 e^{-\alpha t},$$

where  $I_0$  is the incident intensity,  $\alpha$  is the absorption coefficient for the solid hydrogen,  $t$  is the sample thickness, and the transmittances  $T$  are for the interfaces given in Fig. 105.34. After vaporization,

$$I'_t = I_0 T_1^4 T_2^2 T_3'^2;$$

now, let

$$T = \frac{I_t}{I'_t} = T_3^2 \frac{e^{-\alpha t}}{T_3'^2}.$$

Assuming nonabsorbing windows,

$$T_3 = (1 - R_3) \text{ and } T_3' = (1 - R_3'),$$

where

$$R_3 = \frac{(n_2 - n_3)^2}{(n_2 + n_3)^2} \text{ and } R_3' = \frac{(n_2 - 1)^2}{(n_2 + 1)^2}$$

at normal incidence.

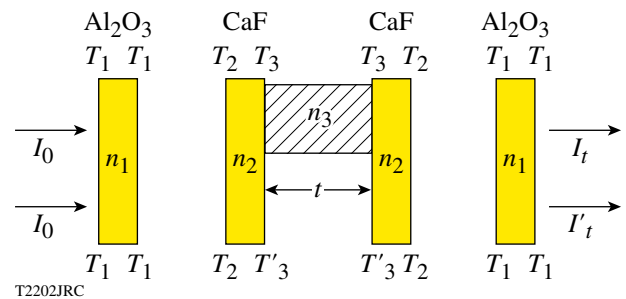


Figure 105.34

The attenuation of the sample beam as it passes through the sample cell with and without the solid hydrogen. Both the increase in absorption from the presence of the solid slab and the reduction in reflectivity at the internal boundaries of the cell's windows due to its presence must be accounted for to obtain an accurate absorption coefficient.

The refractive indices  $n$  are those shown in Fig. 105.34. Letting

$$\beta = \frac{(1 - R'_3)^2}{(1 - R_3)^2},$$

$$T = \frac{e^{-\alpha t}}{\beta} \text{ and } \alpha = -\frac{\ln(\beta T)}{t}.$$

Therefore, by measuring  $I_t$  and  $I'_t$ , taking their quotient  $T$ , and correcting it using  $\beta = 0.964$  at  $\lambda = 3.16 \mu\text{m}$  for these materials, the absorption coefficient can be measured.

#### ACKNOWLEDGMENT

This work was supported by the U.S. Department of Energy Office of Inertial Confinement Fusion under Cooperative Agreement No. DE-FC52-92SF19460, the University of Rochester, and the New York State Energy Research and Development Authority.

#### REFERENCES

1. P. W. McKenty, T. C. Sangster, M. Alexander, R. Betti, R. S. Craxton, J. A. Delettrez, L. Elasky, R. Epstein, A. Frank, V. Yu. Glebov, V. N. Goncharov, D. R. Harding, S. Jin, J. P. Knauer, R. L. Keck, S. J. Loucks, L. D. Lund, R. L. McCrory, F. J. Marshall, D. D. Meyerhofer, S. P. Regan, P. B. Radha, S. Roberts, W. Seka, S. Skupsky, V. A. Smalyuk, J. M. Soures, K. A. Thorp, M. Wozniak, J. A. Frenje, C. K. Li, R. D. Petrasso, F. H. Séguin, K. A. Fletcher, S. Padalino, C. Freeman, N. Izumi, J. A. Koch, R. A. Lerche, M. J. Moran, T. W. Phillips, G. J. Schmid, and C. Sorce, *Phys. Plasmas* **11**, 2790 (2004).
2. F. J. Marshall, R. S. Craxton, J. A. Delettrez, D. H. Edgell, L. M. Elasky, R. Epstein, V. Yu. Glebov, V. N. Goncharov, D. R. Harding, R. Janezic, R. L. Keck, J. D. Kilkenny, J. P. Knauer, S. J. Loucks, L. D. Lund, R. L. McCrory, P. W. McKenty, D. D. Meyerhofer, P. B. Radha, S. P. Regan, T. C. Sangster, W. Seka, V. A. Smalyuk, J. M. Soures, C. Stoeckl, S. Skupsky, J. A. Frenje, C. K. Li, R. D. Petrasso, and F. H. Séguin, *Phys. Plasmas* **12**, 056302 (2005).
3. P.W. McKenty and M.D. Wittman, *Bull. Am. Phys. Soc.* **50**, 115 (2005).
4. I. Prigogine, R. Bingen, and J. Jeener, *Physica (The Hague)* **XX**, 383 (1954); *ibid.* 516; *ibid.* 633.
5. M. Bienfait *et al.*, *Phys. Rev. B* **60**, 11,773 (1999).
6. A. Crane and H. P. Gush, *Can. J. Phys.* **44**, 373 (1966).
7. J. Van Kranendonk, *Solid Hydrogen: Theory of the Properties of Solid  $H_2$ ,  $HD$ , and  $D_2$*  (Plenum Press, New York, 1983), pp. 29–51.
8. L5004-IR Spectrometer System, Laser Components IG, Inc., Hudson, NH, 03051, September 2004, <http://www.lasercomponents.com/www/products/index.html> (8 February 2006).
9. Displex Low Vibration/Mossbauer Cryostat, DMX-20 Interface, Advanced Research Systems, Inc., Macungie, PA, 18062, 2004, <http://www.arscryo.com/dmx20.html> (8 February 2006).
10. J. Van Kranendonk, *Solid Hydrogen: Theory of the Properties of Solid  $H_2$ ,  $HD$ , and  $D_2$*  (Plenum Press, New York, 1983), pp. 105–129.
11. *ibid.* p. 119.
12. W. T. Shmayda, Laboratory for Laser Energetics, private communication (2005).
13. *Metals Handbook: Metallography, Structures, and Phase Diagrams*, 8th ed. (American Society for Metals, Metals Park, OH, 1973), p. 294.
14. G. W. Collins *et al.*, *J. Vac. Sci. Technol. A* **14**, 2897 (1996).
15. D. N. Bittner, Shafer Corporation, private communication (2005).